PHOSPHOLIPID MONOLAYERS BETWEEN FLUID AND SOLID STATES

C. A. HELM,* H. MÖHWALD,* K. KJAER,‡ AND J. ALS-NIELSEN‡
*Physics Department, T.U. Munich, D-8046 Garching, West Germany; and ‡Risø National Laboratory, DK-4000 Roskilde, Denmark

ABSTRACT Monolayers of the phospholipid dimyristoyl phosphatidic acid on the surface of water have been studied by a combination of the new techniques of synchrotron x-ray diffraction and fluorescence microscopy with classical surface pressure data. The pressure vs. area isotherm changes slope at the surface pressures π_c and π_s. The optical technique demonstrates that between π_c and π_s the fluid phase coexists with a denser "gel" phase. Electron diffraction data have shown that the gel phase has bond orientational order over tens of micrometers. However, the x-ray data demonstrate that positional correlations extend only over tens of angstroms. Thus, the gel phase is not crystalline. Above π_s a solid phase is formed with a positional correlation range that is eight times longer for the chemically purest films.

1. INTRODUCTION

Phospholipid monolayers provide simplified model systems of biological membranes (Phillips, 1972): The phase behavior of the monolayer exhibits properties that may be relevant for bilayers as well. Further the monolayers are well-suited for the study of general physical principles concerning ordering processes in two dimensions (Kosterlitz and Thouless, 1973; Nelson and Halperin, 1979). Specifically concerning phospholipids there have been many efforts to theoretically understand the nature of the so-called "main phase transition" from a fluid to a gel state (Forsyth et al., 1977; Georgallas and Pink, 1981). Work concentrated on the orders of one or more phase transitions involved, on the molecular arrangement in different phases, on the underlying forces and on the metastability of the film (Horn and Gershfeld, 1977). Until 1983 experimental data predominantly resulted from measurements of pressure vs. area isotherms (Cadenhead et al., 1980; Albrecht et al., 1978) or from isobars and thus did not directly yield microscopic information. Hence, whereas the sharp break in the slope of the isotherm at the pressure π_c (see Fig. 1 *A*) could unambiguously be assigned to the onset of a fluid/gel main phase transition, the interpretation of the second change of slope at a higher pressure π_s remained controversial. It was ascribed to a second-order phase transition from a crystalline-tilted to a crystalline (Albrecht et al., 1978) or from a liquid-condensed to a solid (Cadenhead et al., 1980) phase. These interpretations obviously differed in the model assumptions of the monolayer state at surface pressures between π_c and π_s.

Much progress in understanding the type of phase transition has been obtained by fluorescence microscopic studies of surface textures evolving on increasing the surface pressure above π_c (Lösche et al., 1983; Peters and Beck, 1983; Weiss and McConnell, 1984).

The images clearly showed coexistence in a first order phase transition between the fluid phase also existing below π_c and a denser phase here denoted the "gel" phase in accordance with convention (Fischer et al., 1984; Lösche and Möhwald, 1984*a*). As this powerful technique did not yield information on the molecular level, monolayers had to be transferred onto solid supports for electron diffraction studies (Fischer and Sackmann, 1984). In this way it was shown that the gel phase has long range bond-orientational order.[1] The first x-ray diffraction experiment on lipid films on a substrate was reported by Seul et al. (1983). In both kinds of experiments, however, the properties of the monolayer might have been substantially altered during transfer (Kopp et al., 1975).

To eliminate this latter drawback we have designed experiments to measure synchrotron x-ray diffraction from a monolayer at the air/water interface (Möhwald, 1986; Kjaer et al., 1987). We report here comprehensively on our results for the phospholipid L-α-dimyristoyl phosphatidic acid (DMPA). We demonstrate that the gel phase formed above π_c exhibits only a very short range of positional order. The positional coherence length increases drastically beyond the surface pressure π_s.

By varying the ionic strenth of the subphase we changed

[1]This was observed with several kinds of substrate surfaces, including amorphous SiO and carbon layers. Further, by polarization fluorescence microscopy it was shown (for dipalmitoyl phosphatidic choline [DPPC]) that monolayers at the air/water interface exhibit long range orientational order (Moy et al., 1986). Bond orientational long range order thus seems to be an intrinsic property of the monolayers in the gel state.

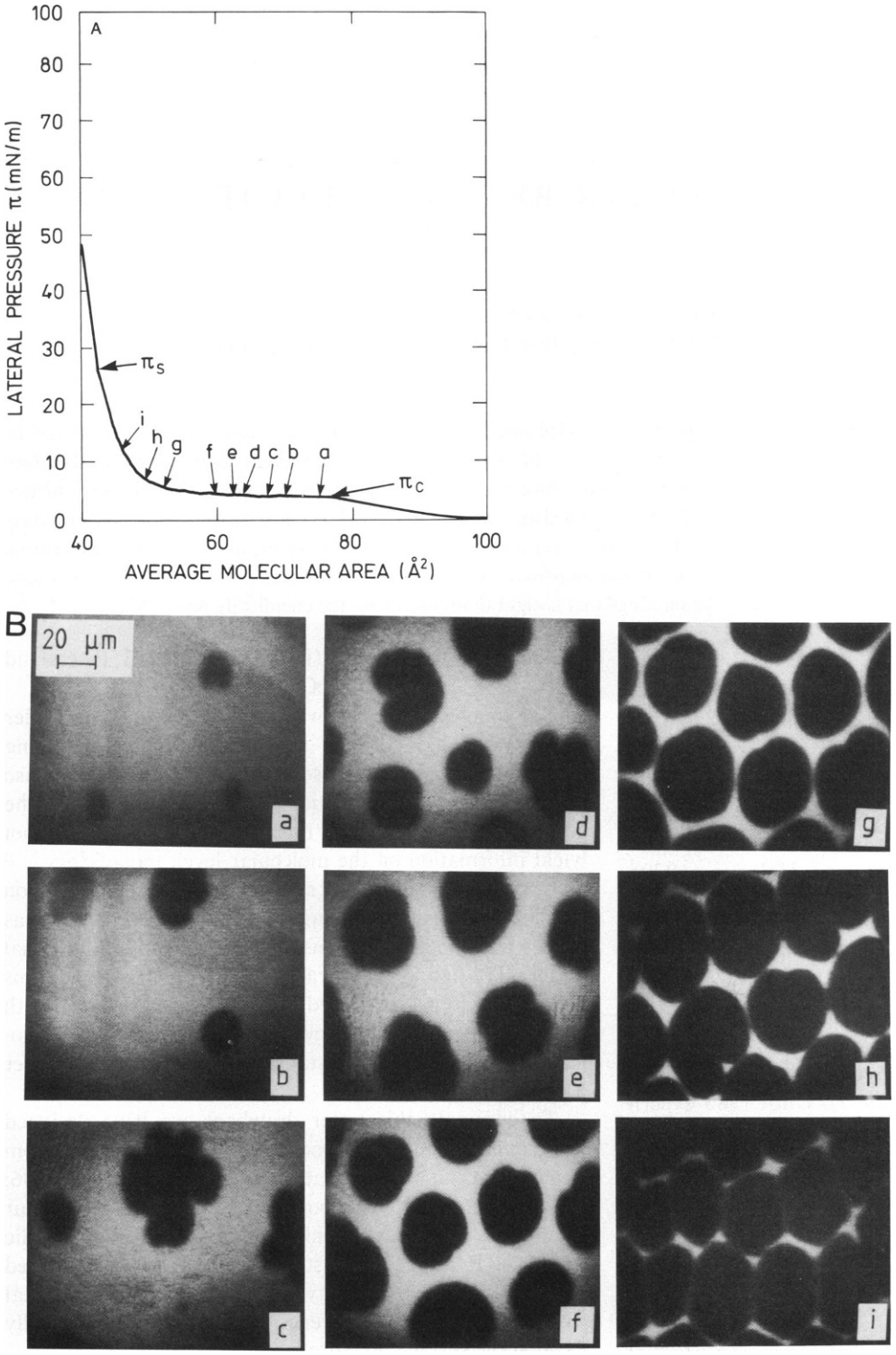

FIGURE 1 (*A*) Pressure–area isotherm (T = 19°C) of DMPA with 1 mol% of the dye DP-NBD-PE and 10^{-4} M NaCl, $5 \cdot 10^{-5}$ M EDTA in the water subphase. (*B*) Fluorescence micrographs at the (A,π) values marked on the isotherm. The light areas are fluid phase, the dark areas gel phase.

the surface charge density and hence π_c and π_s. This demonstrated that the observed features are coupled to these singular points of the pressure vs. area isotherms.

The paper is organized as follows. The next section describes the experimental methods and results obtained from thermodynamic measurements, fluorescence microscopy, and x-ray diffraction.

The latter technique, when applied to a film floating on water, has not been described before. Therefore a detailed description is given. Section 3 deals with the analysis of the results and in Section 4 we discuss our results in the light of knowledge or conjectures on the structure of the solid phase and the gel phase from other experimental techniques and theoretical investigations.

2. EXPERIMENTAL PROCEDURES AND RESULTS

(a) Thermodynamic Measurements

Accurate thermodynamic data for DMPA, obtained on dedicated film balances, have been reported previously (Albrecht et al., 1978; Lösche, 1986; Lösche et al., 1984). Quantitative monolayer deposition behind the moveable barrier gave directly the average area per molecule, A. The surface pressure, π, was measured by a Wilhelmy balance (Gaines, 1966) detecting the differential pulling force on a piece of blotting paper partly submerged in the subphase. These data constitute reference isotherms for the x-ray experiments reported on in Section 2c.

The technical details concerning the sample were the following. The phospholipid, L-α-dimyristoyl phosphatidic acid (Sigma Chemical GmbH, Munich, FRG), was chromatographically pure and spread from a chloroform/methanol (3:1) mixed solvent. The subphase was distilled in Millipore-filtered water (pH = 5.5) containing $5 \cdot 10^{-5}$ M EDTA. The ionic strength was varied by adding NaCl (E. Merck, Darmstadt, FRG).

The pressure–area isotherm depends on temperature and on the head group charge and thereby on the ionic strength in the subphase. Estimates based on Gouy–Chapman theory (Helm et al., 1986) indicate that the head group charge varies from 0.4 e/molecule to 0.9 e/molecule on increasing the Na^+ ionic strength from 10^{-4} to 10^{-2} M.

We have obtained x-ray data at both these ionic strengths and the corresponding pressure–area isotherms are given in Fig. 1 and Fig. 3, respectively.

(b) Fluorescence Microscopy

The film balance used for fluorescence microscopy has been described previously (Lösche and Möhwald, 1984*b*). The objective lens of a microscope is inserted into the bottom of a Teflon trough with movable barrier and a Wilhelmy type pressure measuring system. Optically excited fluorescence of dye molecules incorporated into the lipid monolayer is monitored by a sensitive TV camera attached to the microscope. Textures are observed because the dye probe is less soluble in the more condensed gel phase (dark) compared with the fluid phase (light).

The dye, used in the fluorescence experiments only, was L-α-dipalmitoyl-nitrobenzoxadiazol-phosphatidylethanolamine (DP-NBD-PE), purchased from Avanti Polar Lipids, Inc. (Birmingham, AL) and applied in a concentration of 1.2 mol%. Previous studies have shown (Lösche and Möhwald, 1984*a*) that surface textures as well as pressure vs. area diagrams are barely affected by the dye for these concentrations.

Interfacing the TV camera to a computer affords quantitative analyses of the resulting images (Duwe, 1985).

Observed textures are shown in the lower part of Fig. 1 *B*. The frames correspond to the points indicated on the pressure–area isotherm for $\pi_c < \pi < \pi_s$ (Fig. 1 *A*). It is immediately apparent that two phases coexist in this pressure region. As the pressure is increased, the percentage of lipids in the gel phase increases. Cellular or dendritic textures may occur but partly disappear by annealing (Miller, 1986; Miller et al., 1986). The gel phase domains are rather uniform in size and may form a superlattice due to electrostatic forces (Fischer et al., 1984; Andelman et al., 1985). In the next section we shall analyze the ratio of light areas to dark areas versus pressure in connection with the lever-rule for coexisting phases.

(c) X-Ray Diffraction

We were able to obtain the first x-ray diffraction results from a monolayer film floating on water (Möhwald, 1986). Data taken at various pressures above π_c have been described recently (Kjaer et al., 1987) and are reproduced in Fig. 3 of this paper.

A Langmuir trough with Wilhelmy balance and moveable barrier (Gaines, 1966) can be placed on the sample goniometer of an x-ray diffractometer for horizontal scattering (Fig. 2). The trough is housed in a gas-tight cannister with x-ray transparent windows. The working temperature could be controlled to within 0.1°C by a thermostated waterflow through the copper base of the Teflon trough. The Wilhelmy balance was calibrated using the well-known isotherm of arachidic acid. However, due to drift, the absolute pressures reported here may be too high by as much as 5 mN/m. Further, due to difficulties with achieving a quantitative deposition, as well as occasional leaking under the barrier, the absolute area per

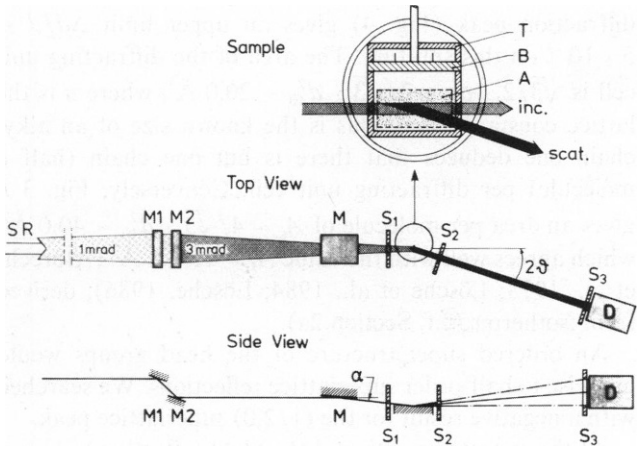

FIGURE 2 Top and side view of the x-ray diffraction geometry. SR denotes the synchrotron radiation beam; M1 and M2 the two Ge(111) monochromator crystals; M denotes a flat, gold-coated mirror; S_1, S_2, and S_3 denote various slits; and D is the NaI scintillation detector. The inset shows the "crossed-beam" definition of the diffracting part of the film area and shows also the Langmuir through T with variable barrier B and a glass plate A to provide a shallow water height.

molecule, A, was not determined exactly. Instead, the areas corresponding to the measured pressures, π, were deduced from the standard π vs. A isotherms described in Section 2a.

However, it was possible to verify the purity of the system by the shapes of the raw π vs. barrier position isotherms. In particular, the kinks at π_c and π_s could be clearly identified.

The monochromatic x-ray beam was incident at a small downwards angle α on the film floating on the water surface. The beam diffracted through the horizontal angle 2θ is defined by the slits S_2 and S_3 so that the diffracting film area is the overlap of the incident and diffracted beams as shown in the inset of Fig. 2.

For a two-dimensional crystalline sample Bragg peaks would result at scattering angles 2θ fulfilling Bragg's law $\lambda = 2d_{hk}\sin\theta$, where as usual λ denotes the x-ray wavelength and d_{hk} the lattice repeat distance with the two-dimensional Miller indices (h, k). A sharp peak was indeed observed, c.f., Fig. 3 *h* and Fig. 4, at a pressure slightly above π_s. The peak intensity remained constant when the Langmuir trough was turned through 60°, showing that the diffracting film area is not a single crystal domain but rather consists of many randomly ordered domains (a two-dimensional powder). The peak position ($2\theta = 19.10°$) together with the wavelength of 1.3815 Å gives a lattice repeat distance of $d_{hk} = 4.163$ Å at $\pi \simeq 40$ mN/m.

Electron diffraction studies (Fischer et al., 1984) on phospholipid monolayers transferred onto a substrate displayed a single crystal-like diffraction pattern of hexagonal symmetry. The d-spacing d_{10} was ~ 4.2 Å. In accordance with these results we assume that the film on the water surface forms a hexagonal lattice as well; and we index the x-ray peak (1, 0). A deviation from hexagonal symmetry would result in a splitting of the peak. Our narrowest diffraction peak (Fig. 4) gives an upper limit $\Delta d/d \leq 5 \cdot 10^{-3}$ on this splitting. The area of the diffracting unit cell is $\sqrt{3}/2 \cdot a^2 = 2/\sqrt{3} \cdot d_{10}^2 = 20.0$ Å^2, where a is the lattice constant. Since this is the known size of an alkyl chain one deduces that there is but one chain (half a molecule) per diffracting unit cell. Conversely, Fig. 3 *h* gives an area per molecule of $A_s = 4/\sqrt{3} \cdot d_{10}^2 = 40.0$ Å^2, which agrees well with the value $A_s = 41 \pm 1$ Å^2 (Albrecht et al., 1978; Lösche et al., 1984; Lösche, 1986), derived from isotherms (c.f. Section 2a).

An ordered superstructure of the head groups would give rise to half-order superlattice reflections. We searched with a negative result for the (1/2,0) superlattice peak.

At the expected position of the (1,1) reflection no signal above the background level was detected. In this connection it is worthwhile noting that a recent electron diffraction study of a Langmuir–Blodgett film of cadmium stearate yielded (1,1) and (2,0) intensities which were only a few percent of the (1,0) intensity (Garoff et al., 1986). On the basis of this we should probably not expect to observe the (1,1) peak because the optimal (1,0) peak in

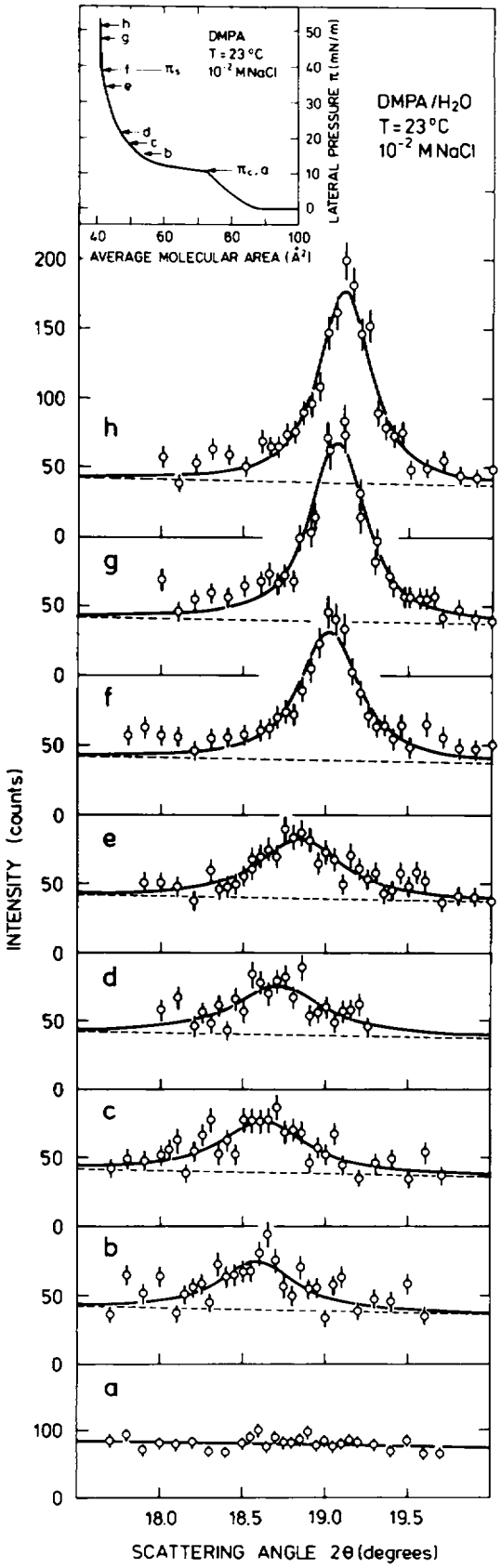

FIGURE 3 Diffracted intensity around the (1,0) peak at various points *a–h* on the isotherm as given in the inset. T = 23°C, pure DMPA film on water subphase with 10^{-2} M NaCl and $5 \cdot 10^{-5}$ M EDTA.

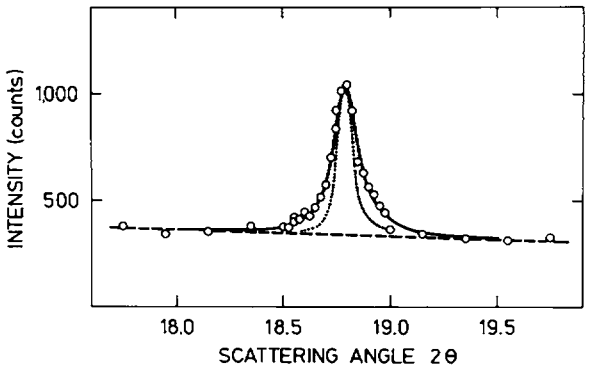

FIGURE 4 High resolution measurement of the line shape in the solid phase. The peak width corresponds to a positional correlation range of almost 100 lattice distances. The dotted line is the resolution as measured by scanning 2θ through the direct beam. The dashed line represents a slightly sloping background.

Fig. 4 indicates that other peaks must not be less than ~10% of the (1,0) peak if they should be visible in the x-ray diffraction pattern at our present level of sensitivity.

As the pressure is lowered from π_s Fig. 3 shows that the (1,0) peak broadens and shifts, and the integrated intensity decreases. The latter effect is caused by loss of diffracting molecules to the fluid phase, c.f., the fluorescence microscopy images in Fig. 1. The peak broadening means that the gel phase is not as well correlated as the solid phase and certainly not crystalline. We shall, however, postpone further discussion of this point to the next section.

We will now describe the technical requirements for obtaining x-ray diffraction patterns as shown in Fig. 3 from a phospholipid monolayer floating on the water subphase. First, the number of molecules in a layer that is only 25-Å thick although ~10 mm^2 in area is fairly small. Second, only a small fraction of the domains are correctly oriented to diffract the monochromatic incoming beam, and third, the two-dimensional nature of the film causes the scattering to be vertically smeared out into a so-called Bragg rod. The detector's vertical aperture accepts only a fraction of this rod. It is therefore necessary to use a very intense x-ray source. The set up shown in Fig. 2 is located at the bending magnet beam line D4.1 of the synchrotron x-ray source DORIS II at HASYLAB, DESY, Hamburg. Furthermore, the monochromatic beam is sagittally focused onto the sample by a curved second monochromator crystal (M2 in Fig. 2).

The signal-to-background ratio is only 3:1 even in the most compressed phase (Fig. 3 *h*). Therefore reduction of the background is of the utmost importance. Ideally, the effective x-ray penetration depth Λ into film and subphase should only slightly exceed the film thickness of 25 Å. The 1/e absorption length ℓ at normal incidence ($\alpha = 90°$) is ~2 mm. Neglecting refraction effects one would have $\Lambda = \alpha\ell/2$ or ~1.75 μm at the applied value of $\alpha = 0.00175$ rad. However, at such small angles refraction effects cannot be neglected. As a matter of fact, the critical angle for total reflection, α_c, is 0.00238 rad at $\lambda = 1.38$ Å, so for $\alpha < \alpha_c$ a so-called evanescent wave is excited below the surface. This wave propagates along the surface and its amplitude decays exponentially with depth.

At the present value of $\alpha/\alpha_c = 0.74$ the effective penetration depth is 75 Å (Als-Nielsen, 1987, Eq. 5.27). For $\alpha \ll \alpha_c$ the penetration depth is simply $\lambda/(4\pi\alpha_c) \simeq 46$ Å. The idea of enhancing surface sensitivity by the use of glancing angles near the critical angle for total reflection was first explored on solid surfaces (Eisenberger et al., 1981). If α/α_c is increased to 1.1, the background in our experiments increases almost a factor of four.

In most of the experiments reported here, the monochromatic beam was reflected by a gold-coated mirror M to the desired angle α with respect to the horizontal liquid surface (c.f. Fig. 2). In other experiments at our set up in HASYLAB (Braslau et al., 1985) we used instead a tilted single crystal monochromator situated between M and S_1 in Fig. 2. Braslau et al. were able to measure the x-ray reflectivity of a pure water surface by using a shallow water depth (a few hundred micrometers) to eliminate mechanically excited long wavelength surface waves. They obtained reflectivities exceeding 95% for $\alpha < \alpha_c$. The high reflectivity as well as the shape of the reflectivity vs. α in the vicinity of α_c verifies that the evanescent beam technique described above is applicable. A glass block (A in Fig. 2) was inserted in the Langmuir trough to obtain a shallow water depth. The actual depth was measured by comparing the x-ray transmission of wavelength λ (water and glass opaque) and of wavelength $\lambda/3$ (water semi-transparent, glass opaque) as the trough was scanned vertically through the horizontal beam.

In later measurement runs, a considerably sharper (1,0) powder diffraction peak was obtained near π_s as shown in Fig. 4. For this experiment an incident beam geometry with a single, tilted monochromator crystal, no mirror, and a 1-mrad Soller collimator in the diffracted beam was used. In all other respects, the setup was identical to that described above and depicted in Fig. 2. When the pressure was decreased into the coexistence region, widths similar to those in *b–e* of Fig. 3 resulted. However, very close to or in the solid phase this sample exhibited a considerably larger correlation range than the other samples. We ascribe the difference in peak widths in the solid phase to a higher chemical purity of the film of Fig. 4.

It was to resolve this longer correlation range that the diffractometer configuration was rebuilt as described.

It is essential to determine the instrumental resolution accurately in order to extract the intrinsic width from the data in Fig. 4. Fortunately the resolution function can be measured by a 2θ scan through the direct beam (Fig. 4, *dotted curve*). This is so because the wavelength spread from perfect crystal monochromators placed in the highly collimated synchrotron beam is negligible in comparison with the angular contributions to the resolution width.

We have also made some kinetic observations. In a

simultaneous recording of (A,π) and the (1,0) peak intensity during compression we found a sharp rise of the intensity within <1 min after the kink at (A_s,π_s) was passed. Leaving this film in the solid phase for a few hours did not change the peak intensity significantly.

Recording the intensity as a function of the horizontal 2θ angle near the Bragg position and simultaneously as a function of the elevation angle of the detector above the horizontal (a so-called Bragg rod scan) yields information about the thickness of the diffracting film. Preliminary data in the solid phase did indeed exhibit a Bragg rod, proving that the diffracted peak around $2\theta = 19°$ is of two-dimensional origin. In the heterogeneous fluid–gel phase coexistence region Bragg rod data would provide information about the thickness of the gel phase islands, whereas specular reflectivity measurements at $2\theta = 0$ (see e.g., Als-Nielsen, 1987) gives the average density profile across the surface. Specular reflection data will be published in future papers (e.g., Helm et al., 1987).

III. ANALYSIS

To obtain quantitative information from diffraction data such as those in Figs. 3 and 4 one must (*a*) assess and subtract the background from the total intensity to obtain the signal intensity, and (*b*) model the signal intensity by a convolution of an assumed, intrinsic line shape with the experimental resolution. The latter is determined empirically by the 2θ lineshape of the direct beam as shown by the dotted line in Fig. 4.

As a reasonable model we assume an asymptotically exponential fall-off in the positional correlation function, $\sim\exp(-r/\xi)$ for large r. The Fourier transform of the correlation function gives the x-ray lineshape. In two dimensions the form is $(q^2 + \xi^2)^{-3/2}$. Upon averaging over all the orientations assumed by the domains within the large diffracting area in the x-ray experiment the "powder-line" shape becomes approximately a simple Lorentzian, $(q^2 + \xi^2)^{-1}$. Here q denotes the difference between the actual wave vector transfer $\mathbf{Q}$ and the reciprocal lattice vector $\mathbf{Q}_o$, i.e.,

$$\mathbf{q} = \mathbf{Q} - \mathbf{Q}_o; \quad q = |\mathbf{q}|; \quad |\mathbf{Q}| = 2k \sin\theta; \quad |\mathbf{Q}_o| = 2\pi/d_{10}. \quad (1)$$

The convolution of the Lorentzian line shape and the empirical resolution function was done numerically. The resulting line shape depends on three parameters: the lattice parameter d_{10}, the correlation range ξ, and the peak intensity. These three parameters were varied in the least squares fitting to the data. A sloping background was inferred in some cases from measurements at low pressures π (e.g., Fig. 3 *a*) and in other cases (Fig. 4) from measurements far away from the peak position in 2θ. We shall now discuss the results for ξ and d_{10} in turn.

Fig. 5 shows the correlation range ξ versus the average molecular area. The open and solid squares derive from two different films at the same nominal conditions in terms of temperature (~20°C) and ionic strength (10^{-2} M NaCl) as discussed in the experimental section. The open circles derive from a film on a 10^{-4} M NaCl subphase. The error bars in Fig. 5 include the errors arising from counting statistics, as propagated through the least squares fitting procedure (Bevington, 1969) and a contribution from the estimated uncertainty in the resolution width.

Not shown in Fig. 3 and 5 are data (or poorer statistics) that seem consistent with a gradual increase in both intensity and correlation range ξ between *a* and *b* of Fig. 3.

The trend is the same for all three films: In the coexistence region the gel phase has a correlation range of not more than about 10 lattice distances. Around (A_s,π_s) the correlation range rises very steeply but the detailed behavior depends on the sample. For the best film the correlation range slightly below A_s is 86 lattice distances.

Our data for the best film (Fig. 4) and solid squares in Fig. 5 have a statistical accuracy making a lineshape analysis meaningful. We have therefore for comparison made least squares fits assuming a Gaussian intrinsic lineshape. Close to π_s the fits of Lorentzians were superior to those of Gaussians. The chi-squared values (Bevington, 1969, Ch. 10) were two to three times larger for the Gaussian than for the Lorentzian lineshape.

Fig. 6 displays the pressure dependence of the peak position converted to *d*-spacing. The reproducibility of the data (from film to film) is governed mainly by purity and also by the experimental uncertainty in the pressure difference $\pi - \pi_s$. Within the scatter of the data one can

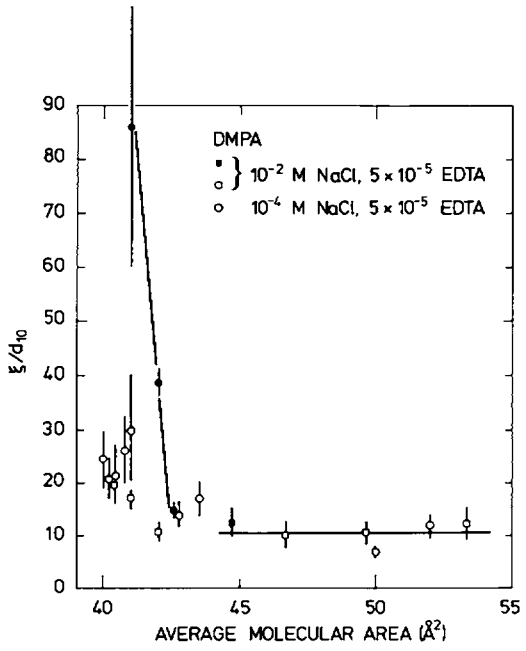

FIGURE 5 The correlation range (relative to the (1,0) *d*-spacing) obtained by fitting a Lorentzian line shape for various film conditions as described in the text.

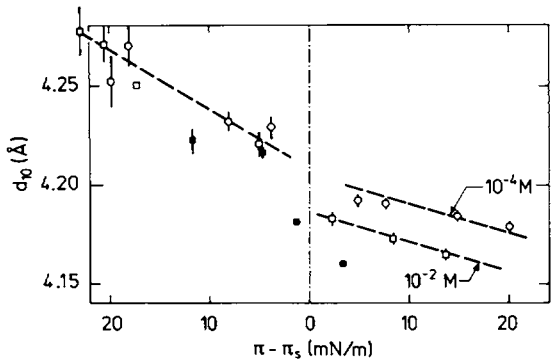

FIGURE 6 Lattice repeat distance versus the pressure deviation from the solidification pressure π_s. The compressibility is estimated from the dashed lines.

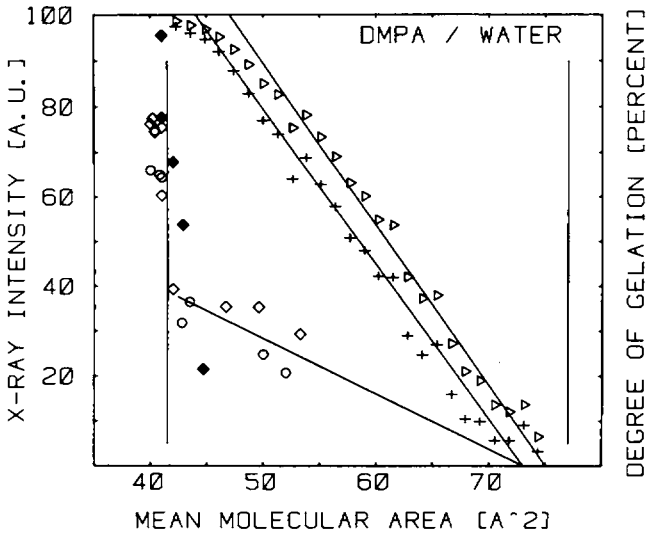

FIGURE 7 Fluorescence microscopy and x-ray intensity data for DMPA, vs. mean molecular area, A. +, relative area of gel phase, ϕ' (dark area in micrographs). Δ, relative number of particles in the gel phase, ϕ. O, ◇, ◆, integrated intensity of the (1,0) x-ray peak. O, 10^{-4} M NaCl. ◇, ◆, 10^{-2} M NaCl. The vertical lines mark the kink points A_c and A_s, as determined from the π vs. A isotherms. The lines through the data points are guides to the eye.

estimate the area compressibility $\kappa = -\delta(\log A)/\delta\pi = -2\delta(\log d_{10})/\delta\pi = (0.7 \pm 0.3) \cdot 10^{-3}$ (mN/m)$^{-1}$ in the solid phase. This is well below the value of $(2.0 \pm 0.2) \cdot 10^{-3}$ (mN/m)$^{-1}$ determined from the slope of the isotherm (Albrecht et al., 1978, 1981). This indicates that the macroscopic compressibility as determined from the isotherms is probably influenced by processes like defect annealing, merging, and deformation of solid domains. We also note that the gel phase becomes more compressible as the spatial correlation range decreases. Finally, the film with by far the longest correlation range below π_s has also the smallest lattice repeat distance. These qualitative features are all consistent with the assumption that the finite correlation range is caused by dislocations so that ξ decreases and κ increases with increasing dislocation densities.

As the coexistence range is traversed, the coexisting gel phase changes simultaneously in both positional ordering range and in density. This change is driven by the pressure rise from π_c to π_s, which would normally not occur during a first order phase transition. The rise in pressure has been discussed in terms of an electrostatic mechanism (Fischer et al., 1984).

The x-ray data in the coexistence region can be used together with the fluorescence micrographs to check the lever-rule for coexisting phases. From the micrographs (Fig. 1 *b*) one can determine the relative amount, ϕ', of dark areas, i.e., the area fraction for the gel phase. Data for ϕ' versus average molecular area A are shown as crosses in Fig. 7.

Also shown are integrated x-ray intensities (*diamonds* and *circles*). The integrated intensity, I, should be proportional to ϕ', to the structure factor $|F|^2$ and to the inverse unit cell area squared,

$$I \propto \phi' \cdot |F|^2 \cdot (d_{10})^{-4}. \tag{2}$$

This assumes that scattering from the fluid phase is seen only as a contribution to the experimental background. The variation due to d_{10} is a small effect and can be ignored. The data in Fig. 7 are consistent with $I \propto \phi'$ in the coexistence region, but the accuracy and range of the intensity data are limited. The sharp increase in intensity beyond A_s must be due to the structure factor and must thus be caused by changes in static or dynamic disorder or in conformation of the alkyl chains. We intend to study this effect further in a future experiment with improved sensitivity. Note that the variation in positional order range, ξ, influences the peak width and peak intensity but not the integrated intensity plotted here.

Next, we consider the mole fraction of the gel phase, ϕ. In terms of molecular areas in the gel phase and fluid phase, A_{gel} and A_{fl}, respectively, and the number of molecules, N_{gel} and N_{fl}, in these phases, one has per definition

$$N \equiv N_{gel} + N_{fl}, \quad NA = N_{gel}A_{gel} + N_{fl}A_{fl}, \quad \phi \equiv N_{gel}/N \tag{3}$$

$$\phi' \equiv N_{gel}A_{gel}/NA = \phi(A_{gel}/A), \tag{4}$$

and also,

$$1 - \phi = (1 - \phi') \cdot (A/A_{fl}). \tag{5}$$

Assuming a constant $A_{fl} = 77$ Å$^2 \simeq A_c$, Eq. 5 was used to derive ϕ, shown as triangles in Fig. 7. We make the following comments on these data: (*a*) The resulting ϕ curve is not strongly dependent on the exact transformation used. Thus, neither the inclusion of a compressibility of the fluid phase nor calculating ϕ through Eq. 4 with the measured x-ray value $4/\sqrt{3} \cdot d_{10}^2$ for A_{gel} will substantially alter the ϕ curve. (*b*) It follows from Eq. 3 that

$$\phi = (A_{fl} - A)/(A_{fl} - A_{gel}), \tag{6}$$

the so-called lever rule for coexisting phases. Thus, a linear variation of ϕ is consistent with constant areas A_{fl}, A_{gel}, which can be determined as the intercepts at $\phi = 0$ and $\phi = 1$, respectively. A straight line can describe the ϕ data in Fig. 7 down to $\sim A = 55$ Å^2. The intercepts are at ~ 75 Å$^2 \simeq A_c$ and at ~ 47 Å^2, which differs by $\sim 15\%$ from the value $A_{gel} = 4/\sqrt{3} \cdot d_{10}^2$ deduced from the x-ray data which extend up to $\sim A = 52$ Å^2. This discrepancy is outside experimental error.

A structural change related to the reorientation of molecular dipole moments may be indicated by surface potential data (Miller, 1986). On compression from a molecular area of 70 Å^2 to 62 Å^2 the potential increases only from 135 to 140 mV for a monolayer of DMPA (pH 5.5, 10^{-3} M ionic strength). Further increase in molecular density then yields a much steeper potential increase towards a value of 350 mV in the solid phase.

DISCUSSION AND CONCLUSIONS

As it is apparent from Fig. 4 the measured lineshape in the solid phase from the most "ideal" film we have been able to obtain is broader than the resolution lineshape. The latter corresponds to a crystallite size of 10^3 Å using the standard Scherrer formula (Guinier, 1963). Since the domain size seen by fluorescence microscopy is larger than 10 μm or 10^5Å we can immediately conclude that the domain cannot be single crystalline. At first sight this may seem to be a surprising result because electron diffraction pictures from a single domain in Langmuir–Blodgett films drawn onto a suitable substrate for such studies unambiguously yield distinct spots of hexagonal symmetry rather than powder rings (Fischer et al., 1984). Further, the orientation of the diffraction pattern did not change by more than 5° over a $\sim$30-μm domain. However, the radial widths of these spots are wider than the electron diffraction resolution, the width being at least $30 \cdot 10^{-3}$ in relative units. Our x-ray diffraction resolution in Fig. 4 is $4.6 \cdot 10^{-3}$ in the same units and the intrinsic width is $3.7 \cdot 10^{-3}$. Thus the Langmuir–Blodgett film yields a width of the (1,0) peak, which is more than ten times broader than the (1,0) peak from the film in the "virgin" state on the water/air interface. The reason may be that the film structure is severely distorted by the transfer from the water/air interface to the substrate. Nevertheless, as mentioned already, the electron diffraction data unambiguously show that the gel phase has bond orientational order over macroscopic distances, whereas the positional order extends only about 10 molecular diameters. A two-dimensional phase with this peculiar type of order has been named "hexatic." It was actually predicted by Nelson (1983) that the solid phase of a phospholipid might be a hexatic glass. In an earlier paper Nelson et al. (1982) examined the two-dimensional packing of equi-diameter hard spheres on a plane when mixed with "impurity" spheres of a different diameter. For certain diameter ratios and impurity concentrations (the locations of the impurities is randomly "frozen in" during the sample preparation) they found indeed the hexactic glass phase. Their paper contains illuminating photographs of planar arrays of spheres with associated dislocation analysis as well as generated structure factors as would be seen in a diffraction experiment. The larger sphere "impurity" could in the phospholipid film correspond to alkyl chains that are not all *trans* and therefore have a correspondingly larger molecular area. The poor reproducibility from film to film in the detailed behavior of ξ may well be consistent with the conjecture that the solid phase is like a hexatic glass, since small differences in chemical purity and preparation of the films may influence the kind of impurities and their concentration.

The influence of impurities on the nature of the monolayer phase transitions has been studied by Pallas and Pethica (1985). As discussed above chemical impurities may be responsible for the limited correlation length in the solid phase. However, we exclude their influence on the correlation length in the gel phase for the following reasons: (*a*) Judged from the models of Nelson et al. (1982) a positional correlation length of nine lattice spacings determined by impurities would require an impurity content of one mol%. This is highly improbable since we generally observe by fluorescence microscopy that the gel phase tends to exclude any molecules different from those of the host matrix. In the opposite case where host and guest molecule differ only slightly ξ would anyway not be affected. (*b*) We may expect varying impurity content in different samples, and this explains the large scatter in the data of ξ in the solid phase. However, there are only small variations in ξ measured at pressures well below π_s with different films. This is compatible with the fact that ξ measured at molecular areas between 45 and 55 Å^2 is an intrinsic property of this phase.

A uniform tilt of alkyl chains would break the hexagonal symmetry observed in the gel and the solid phase, resulting in a splitting of the {1,0} peak. In phospholipid bilayers, such a splitting was observed at high pH by Jähnig et al. (1979). Our data give an upper bound on the deviation from hexagonal symmetry of $5 \cdot 10^{-3}$ in relative units. We have not as yet investigated monolayers at high pH.

A statistical mechanics model for phospholipid monolayers were recently developed by Mouritsen and Zuckermann (1986). This model distinguishes between ordering of the longitudinal configuration in the chains and the positional ordering (in microcrystal-line structure) of the molecules, and for certain choices of interaction parameters two transitions (at π_c and π_s) are identified. However, this model does not imply a longer range of bond orientational order than of positional order in contrast with the electron diffraction data.

In principle, one can distinguish between the microcrystalline model and the hexatic glass model by the lineshape of the (1,0) diffraction peak. The latter implies a Lorent-

zian shape, whereas the Gaussian is traditionally taken to indicate well-ordered crystals of finite size. As mentioned in the previous section our data favor a Lorentzian lineshape.

It is intriguing to speculate on the reason for the discrepancy between (*a*) the gel phase molecular area $A_{gel} \simeq 47$ Å^2 determined by a straight line which fits the ϕ data down to $\sim A \simeq 55$ Å^2 and (*b*) the x-ray data, useful up to $\sim A \simeq 52$ Å^2, which give $A_{gel} \simeq 41$ Å^2. Possibilities which we have considered include (*a*) an extra transition at $A \simeq 54$ Å^2, (*b*) a large amount of fluid phase hidden as invisible islands in the gel phase, or (*c*) a large concentration of vacancies in the gel phase. However, until more data are available we must leave the question open.

To summarize our main results, we have shown that between π_c and π_s the fluid phase coexists with a gel phase which has bond orientational order over tens of micrometers but a positional order range of only a few tens of angstroms. The solid phase formed above π_s has a somewhat longer positional correlation range. Also, the x-ray intensity indicates a reduction of random disorder in the solid phase. The single diffraction peak we have observed argues against the assumption of a large, uniform tilt of the alkyl chains. The microscopic compressibility of the solid phase is less than the macroscopic value. Variation of the subphase shows the association of the kink points π_c and π_s of the pressure vs. area isotherms with the structural changes detected by microscopic and diffraction data to be non-accidental.

We appreciate helpful discussions with O. G. Mouritsen, M. Zuckermann, and E. Sackmann, and the assistance of the staff at HASYLAB. L. A. Laxhuber, F. Grey, R. Feidenhans'l, and M. Nielsen each contributed to the experiments reported on here or to exploratory experiments preceeding them.

This work was supported by the German Bundesministerium für Forschung und Technologie (BMFT) and the Danish Natural Science Foundation.

Received for publication 5 January 1987 and in final form 18 May 1987.

REFERENCES

Albrecht, O., H. Gruler, and E. Sackmann. 1978. Polymorphism of phospholipid monolayers. *J. Phys. (Paris).* 39:301–313.

Albrecht, O., H. Gruler, and E. Sackmann. 1981. Pressure-composition phase diagrams of cholesterol/lecithin, cholesterol/phosphaticid acid, and lecithin/phosphatidic acid mixed monolayers: a langmuir film balance study. *J. Colloid Interface Sci.* 79:319–338.

Als-Nielsen, J. 1987. Solid and liquid surfaces studied by synchrotron x-ray diffraction. *In* Structures and Dynamics of Surfaces. Vol. 2. W. Schommers and P. von Blanckenhagen, editors. Springer Verlag, Berlin.

Andelmann, D., F. Brochard, P. G. de Gennes, and J. F. Joanny. 1985. Physique des surfaces et des interface. Transition des monocuche a molecules polaires. *C. R. Acad. Sci.* 301:675–678.

Bevington, P. R. 1969. Data Reduction and Error Analysis for the Physical Sciences. McGraw-Hill Book Co., New York.

Braslau, A., M. Deutsch, P. S. Pershan, A. Weiss, J. Als-Nielsen, and J. Bohr. 1985. Surface roughness of water measured by x-ray reflectivity. *Phys. Rev. Lett.* 54:114.

Cadenhead, D. A., F. Müller-Landau, and B. M. J. Kellner. 1980. Phase transitions in insoluble one and two-component films at the air/water interface. *In* Ordering in Two Dimensions. Elsevier Biomedical Press, Amsterdam. 73–81.

Duwe, H. P. 1985. Analyse thermisch angeregten Oberflächen-Wellen zur Bestimmung des Elastizitätsmoduls von Membranen durch Bildverarbeitung. Diploma thesis, Technical University of Munich.

Eisenberger, P., and W. C. Marra. 1981. X-ray diffraction study of the Ge(001) reconstructed surface. *Phys. Rev. Lett.* 46:1081.

Fischer, A., and E. Sackmann. 1984. Electron microscopy and diffraction study of phospholipid monolayers transferred from water to solid substrates. *J. Phys. (Paris).* 45:517–527.

Fischer, A., M. Lösche, H. Möhwald, and E. Sackmann. 1984. On the nature of the lipid monolayer phase transition. *J. Phys. Lett.* 45:L785–791.

Forsyth, P. A., S. Marcelja, D. J. Mitchell, and B. W. Ninham. 1977. Phase transition in charged lipid membranes. *Biochim. Biophys. Acta.* 469:335–344.

Gaines, G. 1966. Insoluble Monolayers at Liquid-Gas Interfaces. Ch. 3. John Wiley & Sons, Inc., New York, London, Sidney.

Garoff, S., H. W. Deckmann, J. H. Dunsmuir, M. S. Alvarez, and J. M. Bloch. 1986. Bond orientational order in Langmuir-Blodgett surfactant monolayers. *J. Phys. (Paris).* 47:701–709.

Georgallas, A., and D. A. Pink. 1981. Phase transition in monolayers of saturated lipids. *J. Colloid Interface Sci.* 89:107–116.

Guinier, A. 1963. X-Ray Diffraction in Crystals, Imperfect Crystals and Amorphous Bodies. W. H. Freeman & Co., Publishers, San Francisco, London.

Helm, C. A., L. Laxhuber, M. Lösche, and H. Möhwald. 1986. Electrostatic interactions in phospholipid membranes I: influence of monovalent ions. *Colloid & Polym. Sci.* 264:46–55.

Helm, C. A., H. Möhwald, K. Kjär, and J. Als-Nielsen. 1987. Phospholipid monolayer density distribution perpendicular to the water surface: a synchrotron x-ray reflectivity study. *Europhys. Lett.* In press.

Horn, L. W., and N. L. Gershfeld. 1977. Equilibrium and metastable states in lecithin films. *Biophys. J.* 18:301–310.

Jähnig, F., K. Harlos, H. Vogel, and H. Eibl. 1979. Electrostatic interactions at charged lipid membranes. Electrostatically induced tilt. *Biochemistry.* 18:1399–1408.

Kjaer, K., J. Als-Nielsen, C. A. Helm, L. A. Laxhuber, and H. Möhwald. 1987. Ordering in lipid monolayers studied by synchrotron x-ray diffraction and fluorescence microscopy. *Phys. Rev. Lett.* 58:2224–2227.

Kopp, F., O. P. Fringeli, K. Mühlethaler, and H. H. Günthard. 1975. Instability of Langmuir-Blodgett layers of barium stearate, cadmium arachidate and tripalmitin studied by means of electron microscopy and infrared spectroscopy. *Struct. Mech.* 1:75–96.

Kosterlitz, J. M., and D. J. Thouless. 1973. Ordering, metastability and phase transitions in two-dimensional systems. *J. Phys. (Paris).* C6:1181–1203.

Lösche, M., E. Sackmann, and H. Möhwald. 1983. Fluorescence microscopic study concerning the phase diagram of phospholipids. *Ber. Bunsen-Ges. Phys. Chem.* 87:848–852.

Lösche, M. 1986. Das Phasenverhalten eines Quasi-Zweidimensionalen Dielektrikums an der Elektrolyt/Gas-Grenzfläche. Thesis, Technical University of Munich.

Lösche, M., and H. Möhwald. 1984*a*. Impurity controlled phase transitions of phospholipid monolayers. *Eur. Biophys. J.* 11:35–42.

Lösche, M., and H. Möhwald. 1984*b*. A fluorescence microscope to observe dynamical processes in monomolecular layers at the air/water interface. *Rev. Sci. Instrum.* 55:1968–1972.

Lösche, M., J. Rabe, A. Fischer, B. U. Rucha, W. Knoll, and H. Möhwald. 1984. Microscopically observed preparation of Langmuir-Blodgett films. *Thin Solid Films.* 117:269–280.

Miller, A. 1986. Mikrostruktur von Porphyrin- und Phospholipidmonoschichten. Thesis, Technical University of Munich.

Miller, A., W. Knoll, and H. Möhwald. 1986. Fractal growth of

crystalline phospholipid domains in monomolecular layers. *Phys. Rev. Lett.* 56:2633–2636.

Mouritsen, O. G., and M. J. Zuckermann. 1987. Acyl chain ordering and crystallization in lipid monolayers. *Chem. Phys. Lett.* 135:294–298.

Moy, V. I., D. Keller, H. E. Gaub, and H. M. McConnell. 1986. Long range molecular orientational order in monolayer solid domains of phospholipids. *J. Phys. Chem.* 90:3198–3202.

Möhwald, H. 1986. Microstructure of organic mono- and multilayers. *In* The Physics and Fabrication of Microstructures and Microdevices. M. J. Kelly and C. Weisbuch, editors. Springer Verlag, Berlin, Heidelberg.

Nelson, D. R. 1983. Reentrant melting in solid films with quenched random impurities. *Phys. Rev.* B27:2902–2914.

Nelson, P. R., and B. J. Halperin. 1979. Dislocation-mediated melting in two dimensions. *Phys. Rev.* B19:2457–2484.

Nelson, D. R., M. Rubinstein, and F. Spaepen. 1982. Order in two-dimensional binary random arrays. *Phil. Mag.* A46:105–126.

Pallas, N. R., and B. A. Pethica. 1985. Liquid-Expanded to Liquid-Condensed Transitions in Lipid Monolayers at the Air/Water Interface. Langmuir, Vol. 1, No. 4. 509–513.

Peters, R., and K. Beck. 1983. Translational diffusion in phospholipid monolayers measured by fluorescence microphotolysis. *Proc. Natl. Acad. Sci. USA.* 80:7183–7187.

Phillips, M. C. 1972. The physical state of phospholipids and cholesterol in monolayers, bilayers and membranes. *Progr. Surf. Membr. Sci.* 5:139–221.

Seul, M., P. Eisenberger, and H. M. McConnell, 1983. X-ray diffraction by phospholipid monolayers on single-crystal silicon substrates. *Proc. Natl. Acad. Sci. USA.* 80:5795–5797.

Weiss, R. M., and H. M. McConnell. 1984. Two-dimensional chiral crystals of phospholipids. *Nature (Lond.).* 310:5972–5973.

Wolf, S. Grayer, L. Leiserowitz, M. Lahav, M. Deutsch, K. Kjaer, and J. Als-Nielsen. 1987. Elucidation of the two-dimensional structure of an α-amino acid surfactant monolayer on water using synchrotron x-ray diffraction. *Nature (Lond.).* In press.